Design of Hard Coated Hertzian Contacts for Precision Equipment

Mangudi Varadarajan Kartik and Martin L. Culpepper*
MIT Department of Mechanical Engineering
77 Massachusetts Avenue; Cambridge, MA 02139

The accuracy and repeatability of exact constraint devices rely on the geometric stability of their Hertzian contacts. These contacts act as structural and aligning interfaces, therefore they must bear large loads and maintain stable alignment through repeated engage-disengage cycles. Under these circumstances, the geometry of the contacting elements is prone to change due to wear. When this occurs, the accuracy and repeatability of the alignment interfaces they form degrades. The minimization of wear is therefore of prime importance to the continued advancement of precision alignment devices. This may be accomplished by placing hard coatings on the surface f the contacting elements. In precision applications, the loading of the contacts between these elements results in a ratio of coating thickness to Hertzian contact radius, *t'*, less than 0.1. Stresses within hard coatings for ratios below 0.1 have not been examined in sufficient detail to enable deterministic engineering of hard coated Hertzian contacts. In this paper, we formulate the appropriate relationships by fitting equations to the non-dimensionalized results of multi-parametric Finite element analysis simulations. The relationships link coating stresses to coating characteristics (thickness and material properties) and contact conditions (substrate geometry, material properties and loading). These relationships enable engineers to (1) perform deterministic design of hard coated contacts for precision equipment, (2) to ascertain the sensitivity of coating stresses to changes in design parameters, and (3) to develop rules of thumb for the design of these contacts.

Keywords: Exact constraint, repeatability, fixture, kinematic coupling, exact constraint, hard coating, Hertz contact, stress

1. Introduction and background

1.1. The nature of Hertzian contact interfaces and the need for geometric stability

Discontinuous interfaces are essential and troublesome components of precision hardware. They are essential because they make it possible to (1) form semi-permanent geometric relationships between adjacent components, (2) to couple or decouple the functional characteristics of adjacent components and (3) to couple or decouple flows of mass, momentum and energy between adjacent components. Interfaces are troublesome as they provide more opportunity for the adjacent materials at the interface to wear and change without control. The kinematic chains which define the alignment run through the contacts, therefore nanometer-level alignment requires nanometer-level or better stability of the contact interfaces. Achieving nanometer-level stability of contact geometry (e.g. contacting elements and reference surfaces) has thus become an important issue for next generation precision equipment design.

The focus of this paper is to present design models and rules of thumb which precision engineers may use to design hard coated Hertzian contacts between steel balls and grooves. Hard coating these materials provides contact surfaces with a low coefficient of friction and high surface energy, thereby (1) reducing the energy available (via work performed by friction forces) to change the surface and (2) increasing the energy required to change the surface.

1.2. An example in which stable interfaces are important to alignment performance

Exact constraint fixtures rely on Hertzian contacts to set linearly independent constraints between two bodies which are fixtured with respect to each other. Figure 1 shows a common exact constraint device, a kinematic coupling, which is used to define the relative position (x-y-z), and orientation (θx-θy-θz) of a first and a second component.

*Phone: 617 452 2395; Fax: 617 812 0384; E-mail: culpepper@mit.edu

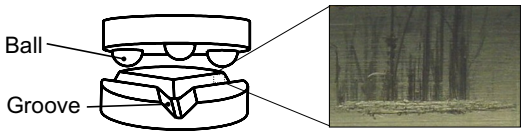

Figure 1: Wear marks on Hertzian contact surfaces in a non-coated precision fixture

Kinematic couplings consist of three convex elements (often referred to as balls) which are rigidly affixed to the first component. The second component is equipped with three concave features (often referred to as grooves) which accept the balls. When the balls are mated in the grooves, the six Hertzian contacts act to constrain six degrees-of-freedom between the first and second body. Hertzian contacts are generally used as they form well-defined constraints that do not act to over constrain the mate. This design has been shown to provide micron-level repeatability as early as the 19th century by Willis, Maxwell and Kelvin [01, 02].

1.3. State of knowledge regarding Hertzian contact design for precision equipment

A common source of non-repeatability and inaccuracy of Hertzian contacts is the wear at the contact areas. The right side of Fig. 1 shows wear marks on a groove surface due to sliding of a ball into and along the groove during centering of the fixture. The wear changes the surface geometry by tens of microns, thereby preventing nanometer-level repeatability. The use of lubricants and ceramic materials for the balls and grooves [03] have been shown to reduced ball-groove wear. Unfortunately, the high-cost and limited ductility of ceramic materials prevents them from being ideal for use in precision couplings. Likewise, lubricants do not provide a general solution as they are not vacuum-compatible and they may not be used in some contamination sensitive applications. Experiments have shown that hard coated steel balls and grooves can provide an alternate solution [04] even though the engineering design of these contacts is not well understood.

1.4. Contents of this paper

In Section 2, we describe how hard coatings may be used to improve the longevity of Hertzian contacts in precision equipment, the specific problems they solve in exact constraint fixtures, and metrics which may be used to ascertain when the models contained herein should be used to design Hertzian contacts. In Section 3 we discuss the failure modes of coated Hertzian contacts. Section 4 describes the simulations, assumptions and dimensionless variables used to develop engineering models. In Section 5 we present a summary of simulation results in graphical form and fit equations to describe the relationship between stress and design parameters. These equations are used in Section 6 to develop rules of thumb and equations which directly relate design parameters to stresses within the coating. The paper closes with a summary of the work in Section 7 and acknowledgements in Section 8.

2. Hard coatings used to provide protection for Hertzian contacts

2.1. Background

Hard coatings may be used to (1) protect and preserves the geometry of the ball-groove contact interface and (2) lower the coefficient of friction between the ball and groove. The former is important as micro and nano-scale wear of the contact interfaces changes the kinematic relationship between the fixtured components, thereby affecting accuracy (long-term wear) and repeatability (short-term wear). The latter is important as lower friction reduces the stick-slip phenomenon [05] which prevents the balls from settling into their lowest energy state within the grooves. This also reduces the amount of energy available at the contact interface to initiate and sustain wear. Previous work has yielded experimental results which indicate that hard-coated Hertzian contacts in kinematic couplings can be used to achieve tens of nanometers repeatability [04]. The anatomy of a hard coated Hertzian contact is shown in Fig. 2.

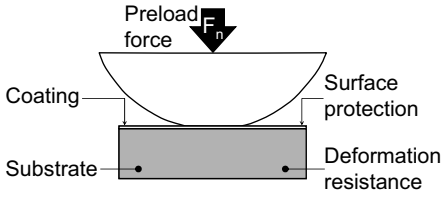

Figure 2: Hertzian contact with protective hard coating over flat substrate

The successful implementation of hard coatings requires an understanding of the relationships between the stresses in the coating, coating design parameters (material properties and thickness), contact characteristics (substrate material properties and substrate geometry) and contact conditions (loads). Unfortunately, there are no guidelines which apply when the ratio of coating thickness to contact radius is less than 0.1. This is a common operating regime for precision equipment as the contacts are highly loaded with the goal of forcing a large contact radius which in produces a high contact stiffness. At the same time, the coating thickness is kept low to reduce fabrication time and cost. At the present, designers must try to intuition their way to a coating design. It is not surprising, that we see some precision equipment designers who "sing the praises of hard coatings" and others have an opposing opinion.

2.2. Benefits for exact constraint devices

Hard coatings are primarily used to preserve the geometry of critical surfaces, for instance bearing races, precision gears, automotive parts, medical devices and cutting tools. Hard coatings are able to do this as they possess high surface energy and a low coefficient of friction. This combination makes it difficult to impart enough energy (via friction forces) to fracture the coating and form new surfaces. In kinematic couplings, the main purpose of the coating is to prevent the wear which occurs before the coupling is fully pre-loaded. For instance, as the balls and grooves engage during coupling, there is relative sliding between them. This is illustrated in Fig. 3. In the Figure, the leftmost diagram shows the balls and groove of the coupling. The bottom balls have already seated into their respective grooves. The top ball is in contact with one groove surface and will slide down into the groove (noted by motion 1) until it makes contact with the other groove surface. The bottom balls slide along their grooves (noted by motions 2) in order to maintain geometric compatibility between the ball and groove patterns.

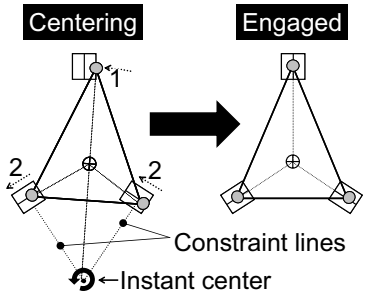

Figure 3: Relative sliding between balls and grooves

As a result, it is typical to obtain the wear marks shown in Fig. 4. The marks are noted as "1" or "2" in keeping with the sliding descriptions of the top and bottom balls respectively.

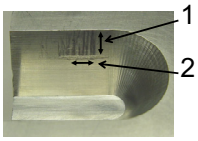

Figure 4: Wear marks on a groove due to ball-groove sliding

As the repeatability of kinematic couplings is coupled with surface finish, it is still necessary to preserve the finish of the contact patches if tens of nanometer repeatability is desired.

2.3. Characteristics of coated contacts in exact constraint devices

The cost of hard coatings and the time required to deposit them limit coating thickness to a few microns. The coating may be orders of magnitude thinner than the substrate, however this is acceptable as the coating is only serving as a protective barrier and does not need to be thick in order to provide contact strength and/or stiffness. Strength and stiffness are determined by the ball and groove substrate material properties and their geometry. Figure 5 shows the coating thickness and contact radius variables in relation to the geometry of the coated joint. The dotted lines in the figure represent the deformed shape of the ball when it is pressed into contact with the flat surface.

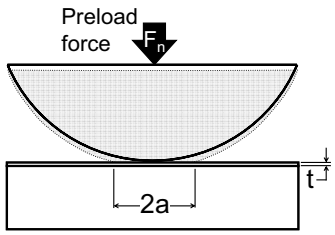

Figure 5: Coating thickness, t, and contact radius, a, for a given preload force, F_n

As noted previously, coating thickness to contact radius ratios less than 0.1 are common in precision equipment. Little work has focused on modeling the behavior of coated interfaces which fit in this regime. Although some approaches have attempted to extrapolate the results for thickness ratios > 0.2 [06, 07] to describe the behavior for thickness ratios 0.1, it can be shown that this approach is incorrect [08]. The lack of appropriate models has led to the current study.

We proceed with the reminder that *hard coatings are meant to protect the surface only, they do not serve to prevent over stressing of the substrate material due to fixturing loads.* This is an important point. In practical applications, the failure stress (shear) in the substrate occurs at a depth below the coating-substrate interface. As such, hardening of the substrate to an appropriate depth, is still required to ensure the integrity of the substrate under large loads.

2.4. Applicability of the theory and models contained in this work

The results of the following work are needed to accurately predict stresses when $t/a < 0.1$. A metric for checking this condition is provided in Eqxn. 1.

$$\frac{t}{a} = t \cdot \left(\frac{4}{3} \cdot \frac{E_e}{R_e} \cdot \frac{1}{F_n \cdot} \right)^{1/3} \leq 0.1 \tag{1}$$

Where F_n is the normal contact force, R_e is given by Eqxn. 2, and E_e, is given by Eqxn. 3..

$$R_e = \left(\frac{1}{R_{ball}} + \frac{1}{R_{groove}} \right)^{-1} \tag{2}$$

$$E_e = \left(\frac{1-\nu_{ball}}{E_{ball}} + \frac{1-\nu_{groove}}{E_{groove}} \right)^{-1} \tag{3}$$

In this work, we have assumed a circular contact patch which results from the contact between a sphere and an axisymmetric groove surface. It is important to note that the material properties of the coating do not appear in the preceding equations. For small coating thicknesses, the size of the contact patch is primarily determined by the contact loading, substrate geometry and substrate material properties [09].

3. Failure modes

The contact of axisymmetric bodies may be represented by an axisymmetric stress field. As such, polar coordinates, r, θ, z, are the easiest to work with when analyzing stresses in the contacting bodies. Figure 6 shows the unit vectors for the polar coordinates which are used in this study.

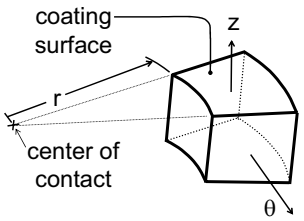

Figure 6: Stresses on a coating element in r, θ, z coordinates

Figure 7 shows the location at which stresses in hard-coated Hertzian contacts are prone to exceed the failure stress of the material. The first subscript on each stress (σ) denotes the direction of the unit normal vector to the face upon which a stress acts. The second subscript denotes the direction of action for the stress. The failure of the substrate is well-known to occur in shear, $\sigma_{rz}|_{z=-0.48a}$, at the center of the contact and a distance of 0.48 a below the surface of the substrate. The stresses of this mode may be predicted using standard Hertzian contact models [09, 10].

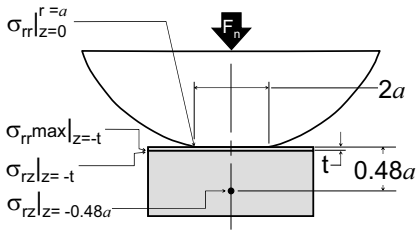

Figure 7: Four failure mode stresses of a coated Hertzian contact; two in the coating ($\sigma_{rr}|_{z=0\ \&\ r=a}$, $\sigma_{rr}max|_{z=-t}$), one at the coating-substrate interface ($\sigma_{rz}|_{z=-t}$) and one in substrate ($\sigma_{rz}|_{z=-0.48a}$)

We are interested in predicting the coating stresses, $\sigma_{rr}|_{z=0\ \&\ r=a}$, $\sigma_{rr}max|_{z=-t}$, and $\sigma_{rz}|_{z=-t}$, shown in Fig. 7. When these stresses exceed a critical limit, failure occurs via one of the modes shown in Fig. 8. Either the radial stress in the coating initiates a circumferential crack (left) or the shear stress at the coating-substrate interface leads to coating-substrate delamination (right).

Figure 8: Failure modes in the coating; circumferential cracking (left) and delamination (right)

In general, the stresses in the circumferential directions, $\sigma_{\theta\theta}$, are compressive and therefore radial cracks are less frequently seen as a mode of failure.

4. Approach used to develop parametric design equations

In our approach, we generate quantitative relationship via the use of dimensional analysis of non-linear FEA results. Similar approaches are commonly used [11, 12, 13, 14] due to the intractable problem of solving the stress field in the vicinity of the contact. In this section, we describe the assumptions used in the model, the important non-dimensional variables, the characteristics of the FEA model and the verification tests which conducted to validate the accuracy of the model.

4.1. Modeling and simulation assumptions

A low coating coefficient of friction (usually 0.1 - 0.2) limits contact friction forces to be small in comparison with the normal force. Based upon this fact and the small dependence of coated contact stresses on tangential loading [10], we are assuming that the contribution of this force to the coating stresses is small compared to those induced by the normal force. The effects of friction have therefore been left as a topic for future study. We also assume perfect geometry of the contacting surfaces as well as a perfectly bonded substrate-coating interface. Material properties are assumed to be linear and isotropic.

4.2. FEA model of coated Hertzian contact

The stresses within the element of larger radius of curvature are more severe, therefore we will restrict this study to stresses within the groove coating. Also, we have already noted that, for small coating thicknesses, the coating does not bear load or provide stiffness which means that its thickness does not affect the deformed shape of the contacting elements. The results of the two preceding sentences lead us to an FEA model which consists of a steel flat with a monolayer coating. An uncoated steel ball is then brought into contact with the coating as a uniformly distributed preload is applied to the ball as shown in Fig. 9. The far-field points in the groove substrate are fully constrained in all directions/orientations. The far-field points in the ball are constrained to move in the z direction only.

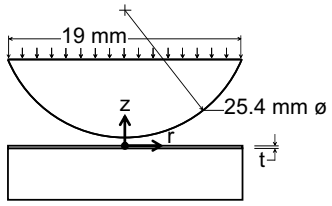

Figure 9: Coated Hertzian contact model

The meshed model contained approximately 70,000 elements. The model size was set to be larger than 30a based upon observations in the literature [15, 16] which show that this is necessary to accurately model the Hertzian stress distributions. A minimum of five elements was maintained across the thickness of the coating.

The characteristics of a non-coated Hertz contact were used to ascertain the accuracy of the FEA model. The model was stripped of its coating layer, loaded while in contact, and the results were compared to traditional Hertzian contact theory. The difference between theory and simulation was found to be less than two percent. A direct comparison of several key contact characteristics is shown in Table 1.

Table.1: Comparison of FEA model and Hertz theory

	$\left.\frac{\sigma_{rr}}{\sigma_{zz}\ \max}\right\|_{r=0}$	$\left.\frac{\sigma_{rr}}{\sigma_{zz}\ \max}\right\|_{r=a}$	$\frac{\sigma_{rz\ principal}}{\sigma_{zz}\ \max}$	$z = z$ at max principle σ_{rz}

Hertz theory	0.790	0.140	0.310	0.480 *a*
FEA	0.778	0.138	0.306	0.473 *a*
% Error	1.5	1.4	1.3	1.5

In addition, the results of this analysis were compared to the published results for $t' > 0.1$. The results match previously reported [15, 16] values to better than 6%.

In the present approach, it is necessary to ascertain the effect of different Poisson's ratios, ν, on the stress state in the coating. Poisson ratios within the range of 0.20 – 0.25 cover most hard metallic and ceramic coatings. Table 2 compares the difference in stress for Poisson ratios 0.20 and 0.25. The results indicate that the effect on the stress state is small enough that the following analysis may be considered valid for hard coatings in which the Poisson's ratio do not vary much from the range of 0.20 – 0.25. Subsequent analyses were carried out for Poisson ratios = 0.25.

Table 2: Stresses at the coating-substrate interface for ν = 0.20 and 0.25

	σ_{rr} $(r = a)$	σ_{zz} $(r = 0)$	$\tau_{max\ (principal\ stress)}$
% Error	3	1	3

4.3. Dimensionless stresses and non-dimensional design parameters

In Table 1, the stresses have been normalized by the maximum normal contact stress, $\sigma_{zz}\ max$. As indicated in Eqxn. 4, $\sigma_{zz}\ max$ is the maximum contact stress on the surface and at the center of the contact patch.

$$\sigma_{zz}\ \max = \sigma_{zz}\Big|_{z=0}^{r=0} \tag{4}$$

The formal representation for our non-dimensionalized stresses, σ_{ij}', is given in Eqxn. 5. The first subscript denotes the direction of the unit normal vector to the face upon which a stress acts. The second subscript denotes the direction of action for the stress.

$$\sigma_{ij}' = \frac{\sigma_{ij}}{\sigma_{zz}\ \max\Big|_{z=0}^{r=0}} \tag{5}$$

We introduce a dimensionless variable for thickness in Eqxn. 6,

$$t' = \frac{t}{a} \tag{6}$$

and the dimensionless Young's Modulus ratio given in Eqxn. 7.

$$E' = \frac{E_c}{E_s} \tag{7}$$

In Eqxn. 7, E_c is the coating modulus and E_s is the modulus of the substrate.

5. Summary of simulation and parametric fit/modeling results

5.1. Quantitative form relating non-dimensionalized stresses and design parameters

Analysis of the data showed that dimensionless stresses and dimensionless variables could be accurately represented by an engineering model of the form shown in Eqxn. 8.

$$\sigma_{ij}'\Big|_z^r = \xi_{1ij}\cdot\left(\frac{t}{a}\right)^{\alpha_{1ij}}\left(\frac{E_c}{E_s}\right)^{\beta_{1ij}} + \xi_{2ij}\cdot\left(\frac{t}{a}\right)^{\alpha_{2ij}}\left(\frac{E_c}{E_s}\right)^{\beta_{2ij}} \tag{8}$$

The sensitivity of the non-dimensionalzed stresses may be calculated using relationships of the form shown in Eqxns. 9 and 10.

$$\frac{\partial\sigma_{ij}'\Big|_z^r}{\partial E_c/E_s} = \psi_{1ij}\cdot\left(\frac{t}{a}\right)^{\alpha_{1ij}}\left(\frac{E_c}{E_s}\right)^{\gamma_{1ij}} + \psi_{2ij}\cdot\left(\frac{t}{a}\right)^{\alpha_{2ij}}\left(\frac{E_c}{E_s}\right)^{\gamma_{2ij}} = \frac{\partial\sigma_{ij}'\Big|_{z'}^{r'}}{\partial E'} \tag{9}$$

$$\frac{\partial\sigma_{ij}'\Big|_z^r}{\partial t/a} = \chi_{1ij}\cdot\left(\frac{t}{a}\right)^{\phi_{1ij}}\left(\frac{E_c}{E_s}\right)^{\beta_{1ij}} + \chi_{2ij}\cdot\left(\frac{t}{a}\right)^{\phi_{2ij}}\left(\frac{E_c}{E_s}\right)^{\beta_{2ij}} = \frac{\partial\sigma_{ij}'\Big|_{z'}^{r'}}{\partial t'} \tag{10}$$

5.2. Simulated and fitted results

The purpose of the following sub-sections is to briefly present the results of the simulations in graphical form and compare these results to the fit provided by the models which are based upon the form of Eqxn. 8. Discussion of the results will be provided in Section 6.

Tensile radial stress in the coating, at the surface, and at the edge of contact

The results of FEA simulations and the fitted representation of the stresses are shown in Fig. 10. These stresses are relatively constant with *t'*, but differ noticeably with *E'*. Both characteristics are captured by the model. The model shows an average error of less than 1.2% for the population of simulated data. The maximum percent error between simulated and fitted data was +8.0%. This error occurs at *t'* = 0.025 and *E'* = 1.0.

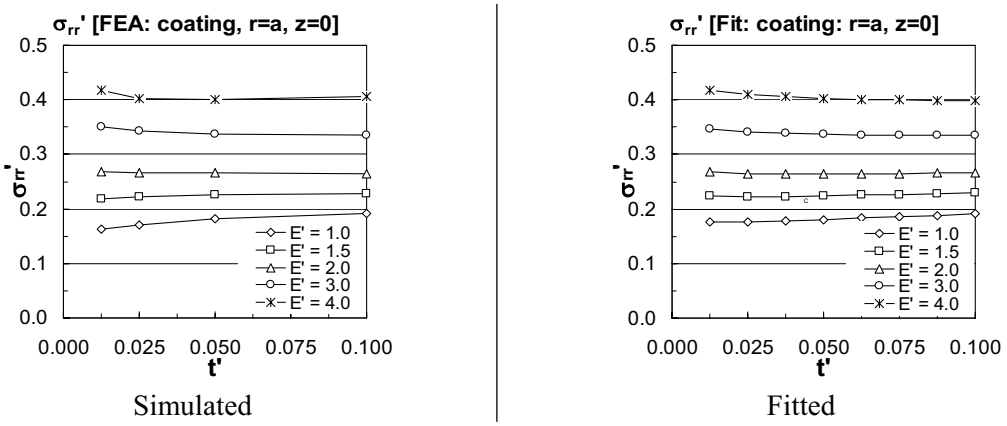

Figure 10: Radial stress, σ_{rr}', in coating at the surface and edge of contact

Equations 11–13 provide the fitted stress relationship and the derivatives of the stress with respect to the independent, dimensionless variables.

$$\sigma_{rr}'\Big|_{z=0}^{r=a} = 0.141\cdot\left(t'\right)^{-0.038}\left(E'\right)^{0.656} + 0.188\cdot\left(t'\right)^{0.709}\left(E'\right)^{-0.633} \tag{11}$$

$$\frac{\partial\sigma_{rr}'\Big|_{z=0}^{r=a}}{\partial E'} = 0.093\cdot\left(t'\right)^{-0.038}\left(E'\right)^{-0.344} - 0.119\cdot\left(t'\right)^{0.709}\left(E'\right)^{-1.633} \tag{12}$$

$$\frac{\partial\sigma_{rr}'\Big|_{z=0}^{r=a}}{\partial t'} = -0.005\cdot\left(t'\right)^{-1.038}\left(E'\right)^{0.656} + 0.133\cdot\left(t'\right)^{-0.291}\left(E'\right)^{-0.633} \tag{13}$$

Maximum tensile radial stress in coating and at coating-substrate interface

The comparison in Fig. 11 shows that these stresses have a strong dependence on *t'* and a weak dependence on *E'* for *t'* larger than 0.05. The model shows an average error of less than 2.8 % for the population of simulated data. The maximum percent error between simulated and fitted data was +10.6%. This error occurs at *t'* = 0.05 and *E'* = 4.0. It is important to note that the maximum radial stress at the substrate interface is always less than the radial tensile stresses at the coating surface. We have included the radial stress at the interface as the coating material properties at this location are often inferior to those of the bulk coating. As such, the inclusion of this stress will offer another analysis tool for designers who have access to the appropriate failure stress data. This issue will be discussed further in Section 6.

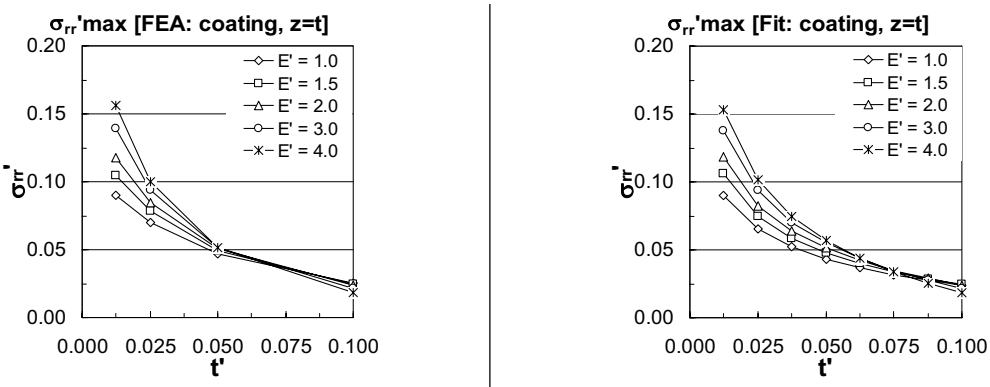

Simulated Fitted

Figure 11: Maximum radial stress, $\sigma_{rr}'max$, in coating at coating-substrate interface

Equations 14–16 provide the fitted stress relationship and the derivatives of the stress with respect to the independent, dimensionless variables.

$$\sigma_{rr}'\max\Big|_{z=-t} = 0.125\cdot\left(t'\right)^{-0.172}\left(E'\right)^{0.526} - 0.148\cdot\left(t'\right)^{-0.040}\left(E'\right)^{0.591} \tag{14}$$

$$\frac{\partial\sigma_{rr}'\max\Big|_{z=-t}}{\partial E'} = 0.066\cdot\left(t'\right)^{-0.172}\left(E'\right)^{-0.474} - 0.088\cdot\left(t'\right)^{-0.040}\left(E'\right)^{-0.409} \tag{15}$$

$$\frac{\partial\sigma_{rr}'\max\Big|_{z=-t}}{\partial t'} = -0.022\cdot\left(t'\right)^{-1.172}\left(E'\right)^{0.526} + 0.006\cdot\left(t'\right)^{-1.040}\left(E'\right)^{0.591} \tag{16}$$

Maximum shear stress at coating-substrate interface

The comparison in Fig. 12 shows that these stresses have a strong dependence on both *t'* and *E'*. The model shows an average error of less than 1.8 % for the population of simulated data. The maximum percent error between simulated and fitted data was +8.9%. This error occurs at *t'* = 0.1 and *E'* = 4.0.

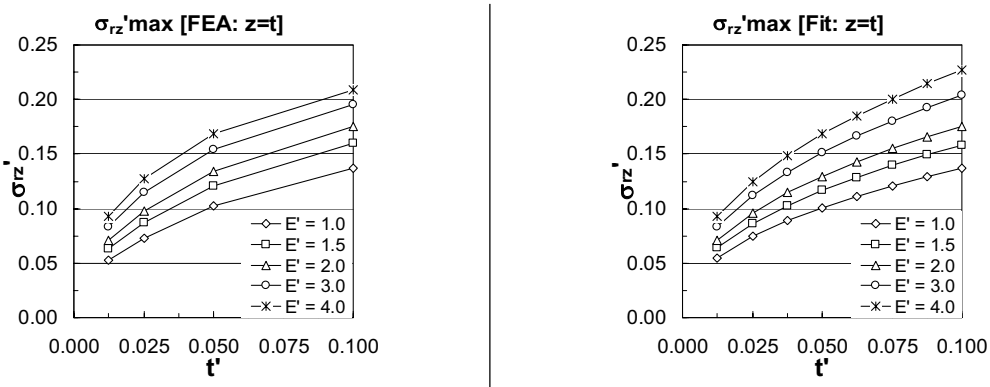

Simulated Fitted

Figure 12: Maximum shear stress, σ_{rz}', between substrate and coating

Equations 17–19 provide the fitted stress relationship and the derivatives of the stress with respect to the independent, dimensionless variables.

$$\sigma_{rz}'\max\big|_{z=-t} = 0.339\cdot(t')^{0.424}(E')^{0.394} + 0.055\cdot(t')^{0.749}(E')^{-0.264} \tag{17}$$

$$\frac{\partial\sigma_{rz}'\max\big|_{z=-t}}{\partial E'} = 0.134\cdot(t')^{0.424}(E')^{-0.606} - 0.014\cdot(t')^{0.749}(E')^{-1.264} \tag{18}$$

$$\frac{\partial\sigma_{rz}'\max\big|_{z=-t}}{\partial t'} = 0.144\cdot(t')^{-0.576}(E')^{0.394} + 0.041\cdot(t')^{-0.251}(E')^{-0.264} \tag{19}$$

6. Design guidelines and models

The purpose of this section is to distill the preceding database of points (σ_{ij}', *t'*, *E'*) and the fitted models into a form which is useful for designers. We first examine the results from a qualitative perspective in order to obtain a sense of how the stresses and non-dimensional variables depend upon each other. We will then transform the quantitative models from the previous section into forms which directly link the true stresses to the characteristics of the coating, the design of the contacting elements and the contact pre-loading.

6.1. Qualitative assessment of simulation results

The results of the simulation may be summed up in the following observations:

1. To reduce the tensile radial stresses on the coating surface – reduce *E'*

2. To reduce the tensile radial stresses in the coating and at the coating-substrate interface – reduce *E'* and increase *t*'

3. To reduce shear stresses at the coating-substrate interface, reduce *E'* and reduce *t*'

This qualitative assessment shows that there will be a conflict between observations two and three if the failure of the coating occurs due to radial stresses at the coating interface rather than the radial stresses at the coating surface. This would happen for instance if the magnitude of the radial failure stress was much lower at the coating-substrate than at the coating surface. The propensity for coatings to have inferior material properties at the interface was discussed in the preceding section.

The conflict is resolved if the ratio of Eqxns. 14 to 11 is smaller than the ratio of the radial failure stress at the coating-substrate interface to the radial failure stress at the coating surface. This condition is described by Eqxn. 20.

$$\frac{\sigma_{rr}'\big|_{z=-t}}{\sigma_{rr}'\big|_{z=0}^{r=a}} = \frac{\sigma_{rr}\big|_{z=-t}}{\sigma_{rr}\big|_{z=0}^{r=a}} = \frac{0.125\cdot(t')^{-0.172}(E')^{0.526} - 0.148\cdot(t')^{-0.040}(E')^{0.591}}{0.141\cdot(t')^{-0.038}(E')^{0.656} + 0.188\cdot(t')^{0.709}(E')^{-0.633}} \le \frac{\sigma_{rr-failure}\big|_{z=-t}}{\sigma_{rr-failure}\big|_{z=0}^{r=a}} \tag{20}$$

Given the state of coating science, and the inherent variation in the coating process, it is not possible to analytically predetermine coating-substrate shear strength. It is best to contact a coating vendor/manufacturer too obtain values (experimental and experience-based) for substrate failure stresses. Note the difference is a strong function of substrate material, coating material and coating process parameters/variation.

6.2. Quantitative assessment of true stresses

From dimensionless stresses to true stresses

Equations 11, 14 and 17 may be transformed to directly link true stresses to the characteristics of the coating, the design of the contacting elements and the contact loading. From Equation 5, we remember that each stress is non-dimensionalzed by the maximum normal contact stress. This stress is given in terms of the contact characteristics (geometry and material properties) and contact conditions (loading) by Eqxn. 21 [10].

$$\sigma_{zz}\max = \sigma_{zz}\big|_{z=0}^{r=0} = \left[F_n\cdot\frac{6}{\pi^3}\cdot\left(\frac{E_e}{R_e}\right)^2\right]^{1/3} \tag{21}$$

We also know that the contact radius for axisymmetric Hertzian contacts may be determined via Eqxn. 22.

$$a = \left[\frac{3}{4}\cdot\frac{R_e}{E_e}\cdot F_n\right]^{\frac{1}{3}} \tag{22}$$

Equations 21 and 22 may then be substituted into Eqxns. 11, 14, and 17 to provide relationships for the true stresses. The relationships are given in Eqxns 23 – 25.

$$\sigma_{rr}\big|_{z=0}^{r=a} = 0.081\cdot t^{-0.038}\cdot F_n^{\,0.346}\cdot\left(\frac{E_e}{R_e}\right)^{0.654}\cdot\left(\frac{E_c}{E_s}\right)^{0.656} + 0.116\cdot t^{0.709}\cdot F_n^{\,0.097}\cdot\left(\frac{E_e}{R_e}\right)^{0.903}\cdot\left(\frac{E_c}{E_s}\right)^{-0.633} \tag{23}$$

$$\sigma_{rr}\max\big|_{z=-t} = 0.072\cdot t^{-0.172}\cdot F_n^{\,0.391}\cdot\left(\frac{E_e}{R_e}\right)^{0.609}\cdot\left(\frac{E_c}{E_s}\right)^{0.526} - 0.085\cdot t^{-0.040}\cdot F_n^{\,0.347}\cdot\left(\frac{E_e}{R_e}\right)^{0.653}\cdot\left(\frac{E_c}{E_s}\right)^{0.591} \tag{24}$$

$$\sigma_{rz}\max\big|_{z=-t} = 0.204\cdot t^{0.424}\cdot F_n^{\,0.192}\cdot\left(\frac{E_e}{R_e}\right)^{0.808}\cdot\left(\frac{E_c}{E_s}\right)^{0.394} + 0.034\cdot t^{0.749}\cdot F_n^{\,0.084}\cdot\left(\frac{E_e}{R_e}\right)^{0.916}\cdot\left(\frac{E_c}{E_s}\right)^{-0.264} \qquad (25)$$

Graphical representation of true stresses

Eqxns. 23 – 25 are plotted within Fig. 13 in triplicate. Each row shows how the respective stresses vary as a function of changes in F_n, t, and R_e. The figure is constructed such that one may see the effects of changing one of the three variables (column) on a specific stress (row).

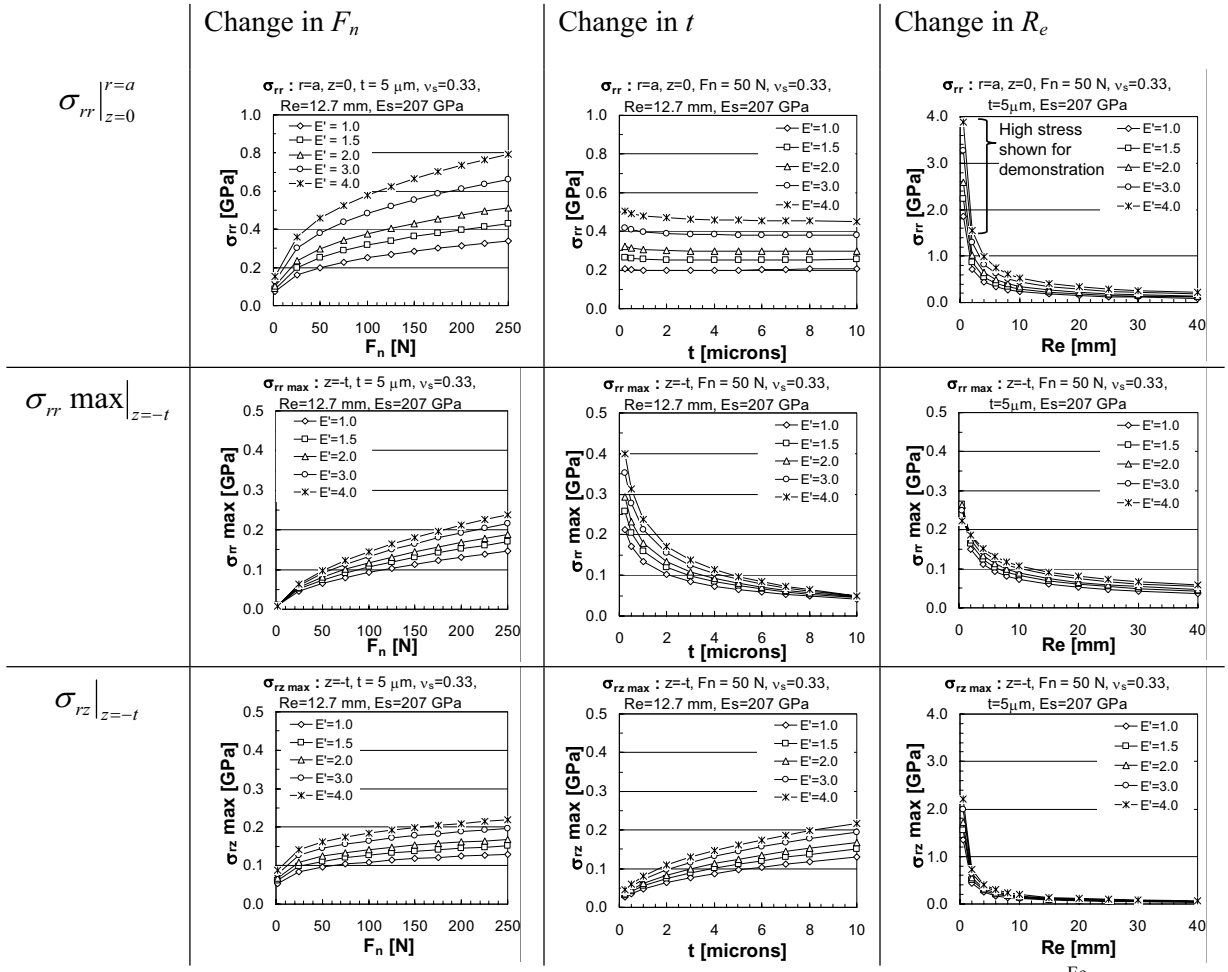

Figure 13: Dependence of failure stresses on design parameters F_n, t, R_e; and the ratio of $^{Ec}/_{Es}$. Note, 1 GPa ~ 145 kpsi

The plots were generated by an Excel™–based, parametric design tool which is posted at http//:psdam.mit.edu/. The plots are helpful to designers in identifying coating thickness, t, coating modulus, E_c, and contact conditions (F_n and R_e) which provide (1) acceptable stress levels and (2) low variation in stresses with variation in design parameters. For instance, designers may use the tool to obtain plots such as those in Fig. 13. They may then select design parameters which place the design performance on the charts at locations of acceptable stress and locations of lower slope (sensitivity) in the curves. In all of the plots, stresses are higher for higher modulus coatings (higher values of E'). This figure enables one to make the following observations:

A. Effect of changing F_n: From Fig. 13, it is possible to see that the magnitude of the stresses increases at a slower rate as one increases F_n. This is expected as the contact area grows with an exponent greater than unity.

Effect of changing t: The radial stress, σ_{rr}, on the surface of the coating and at the edge of the contact is essentially constant with coating thickness. This was not expected and the result has been checked several times for accuracy. The hypothesis used to explain this result is that the radial stresses at the coating surface (for $t/a < 0.1$) depend only on the deformed shape of the coating surface. The deformed shape of the surface is primarily a function of the substrate properties and contact characteristics (R_e and E_e). The coating thickness and properties have little effect on the surface shape due to the fact that they are not responsible for the resistance of the coated surface to deformation from the original shape. In essence, the coating is so thin that its ability to resist deformation and thereby affect the deformed surface shape is limited. In sum, this means that the radial stress at $r = a$ and $z = 0$ should have a weak dependence on t. This insensitivity is welcome as coating thickness is not always easily controlled.

On the other hand, the maximum radial stress in the coating at the coating-substrate thickness is dependant upon coating thickness via coupling through σ_{rz} . The shear stress, σ_{rz}, at the interface grows with increasing thickness. This can be understood by considering that the differential strain between the coating and substrate would be expected to grow as the coating thickness increases. This essentially leads to either the substrate or coating wanting to deform more in the radial direction than its counterpart. The differences in resistance to expansion leads to the increased shear stress between the layers and therefore the dependence of σ_{rr} on t near the coating-substrate interface.

Effect of changing R_e: The contact patch area increases for constant F_n as R_e increases. This leads to broader distribution of the strain energy at the contact and therefore the stresses would be expected to be lower as R_e increases.

7. Summary

In this paper we have provided a database of simulated points which link the geometric and material properties of hard coatings with the stress state in the coating. The relationships apply to common precision design situations in which the ratio of contact thickness to contact patch radius is less than 0.1. Dimensional analysis has been used to distill this data set into a set of models which capture these relationships in a quantitative form. The data and models provide qualitative and quantitative understanding which can be used to make decisions when designing/optimizing precision, hard coated Hertzian contacts. A design tool which includes the results of this analysis has been developed and posted at http://psdam.mit.edu for use by the general precision engineering community. Work on the modeling of hard coated Hertzian contacts is continuing in an effort to incorporate the effects of friction upon coating stress within the model.

8. Acknowledgements

This material is based in-part upon work supported by the National Science Foundation under Grant No. 0348242. We would also like to thank the Ford-MIT alliance for monetary and technical assistance and the Army Research Office for their financial support.

9. References

[01] Maxwell, J.C. "General Considerations Concerning Scientific Apparatus", The Scientific Papers of James Clerk Maxwell, ed. W.C. Nivens, Dover Press, 1890.

[02] Evans, C., “Precision Engineering: an Evolutionary View,” Cranfield Press, Cranfield, Bedford, UK, 1989.

[03] Slocum AH, Donmez A. Kinematic couplings for precision fixturing- Part 2: Experimental determination of repeatability and stiffness. Prec Eng 1988;10;115-22.

[04] Culpepper, M.L., A.H. Slocum, Bailey, P., and Dibiaso, C.M. "Design of detachable precision fixtures, which utilize hard and lubricant coatings to mitigate wear and reduce friction hysteresis." Proceedings of ASPE 18th Annual Meeting.

[05] Hale, LC. and Slocum, AH., Optimal design techniques for kinematic couplings, Prec Eng, April 2001, vol. 25, No. 2, 114-27.

[06] Souza, R.M., Mustoe, G.G.W. and Moore, J.J. "Finite Element modeling of the stresses, fracture and delamination during indentation of hard elastic films on elastic-plastic soft substrates." Thin Solid Films 2001; 392:65-74.

[07] Abdul-baqi, A. and Giessen, E.V. "Indentation-induced interface delamination of a strong film on a ductile substrate." Thin Solid Films 2001; 381: 143-154.

[08] Mangudi V., K., Design of Ultra-Precision Fixtures for Nano-Manufacturing, MIT M.S.M.E Thesis, Cambridge, MA, February 2005.

[09] Mencik, J. Mechanics of Components with Treated or Coated Surfaces. Kluwer Academic Publishers; 1996.

[10] Johnson KL. Contact mechanics. Cambridge, United Kingdom. Cambridge University Press. 1985. pp. 85-9.

[11] Bhowmick, S., Kale, A.N., Jayaram, V. and Biswas, S.K. "Contact damage in TiN coatings on steel." Thin Solid Films 2003; 436: 250-258.

[12] Michler, J. and Blank, E. "Analysis of coating fracture and substrate plasticity induced by spherical indenters: diamond and diamond-like carbon layers on steel substrates." Thin Solid Films 2001; 381: 119-134.

[13] Souza, R.M., Mustoe, G.G.W. and Moore, J.J. "Finite Element modeling of the stresses, fracture and delamination during indentation of hard elastic films on elastic-plastic soft substrates." Thin Solid Films 2001; 392:65-74.

[14] Abdul-baqi, A. and Giessen, E.V. "Indentation-induced interface delamination of a strong film on a ductile substrate." Thin Solid Films 2001; 381: 143-154.

[15] Djabella, H. and Arnell, R.D. "Finite element analysis of the contact stresses in an elastic coating on an elastic substrate." Thin Solid Films 1992; 213: 205-219.

[16] Djabella, H. and Arnell R.D. "Finite element analysis of the contact stresses in elastic double-layer systems under normal load." Thin Solid Films 1993; 223: 98-108.